SAR-Controlled Adaptive Off-Time Technique Without Sensing Resistor for Achieving High Efficiency and Accuracy LED Lighting System

Chao-Hsuan Liu, Chun-Yu Hsieh, Yu-Chiao Hsieh, Ting-Jung Tai, and Ke-Horng Chen, *Senior Member, IEEE*

***Abstract*—A successive approximation register (SAR) is utilized to control adaptive off-time in order to regulate accurate light-emitting diode (LED) current and improve efficiency of LED driver. The proposed SAR-controlled adaptive off-time technique without the external sensing resistor can sense the current flowing through LEDs during the turning on of the N-type power MOSFET, as well as provide adaptive off-time depending on the input voltage and the numbers of LED, to obtain an accurate LED current. Experimental results show the inductor current ripple is kept within $\pm 15\%$ of the DC current. As a result, line regulation is guaranteed in this proposed design.**

***Index Terms*—Adaptive off-time, hysteretic current control (HCC), on-chip low-side current sensing, peak current control (PCC), pulsewidth modulation (PWM) dimming, successive approximation register (SAR).**

I. Introduction

LIGHT-EMITTING diode (LED) lighting systems become more and more popular nowadays because of its many advantages such as low power consumption and long usage lifetime [1]. In addition, LED does not contain infrared and ultraviolet rays in its optical spectrum. That is, it only generates minimal heat and harmful radiation making it environmentally friendly. As depicted in Fig. 1, LED lighting systems can be used on large billboards, traffic lights, streetlamps, backlighting devices [2]–[4], and other similar applications. Furthermore, it is very convenient to control the brightness that depends on the current flowing through LEDs. Recently, automotive electric devices with LED displays have become very popular. Thus, a high efficiency and accuracy LED driving circuit is needed in order to get an accurate control on LED brightness.

The variation of the LED forward voltage can be observed from different manufacturing companies due to the process variation and the I-V curves of LEDs shown in Fig. 2. In addition, the forward voltage also varies depending on the temperature and usage time. With different forward voltages, it is impossible to get uniform brightness by means of the constant voltage control method for these LEDs. The regulated driving current technique becomes the possible and suitable method to drive the LEDs with different forward voltages to get uniform brightness [5]. To control the brightness of the LED lighting system, the current regulator for driving LEDs in series is utilized to ensure the uniform display of the LED array. The design of the LED lighting system needs the regulated driving current technique to flow through the LEDs for uniform brightness. The prior arts of the LED driver are the hysteretic current control (HCC) and peak current control (PCC) techniques. The HCC technique uses two threshold currents to define the average LED current. While it has the advantage of high accuracy, it needs the external sensing resistor in series with the LEDs to achieve it. Contrarily, the PCC technique uses a constant off-time to reduce the need for the connection of the sensing resistor in series with the LEDs, sacrificing the accuracy. The PCC technique connects the sensing resistor at the source node of the N-type

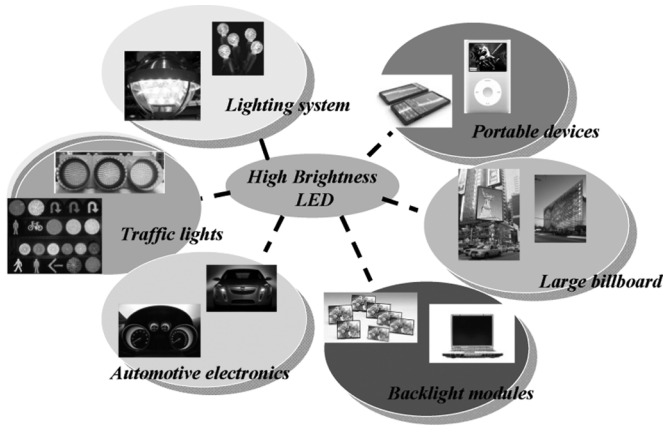

Fig. 1. Applications of LED lighting systems.

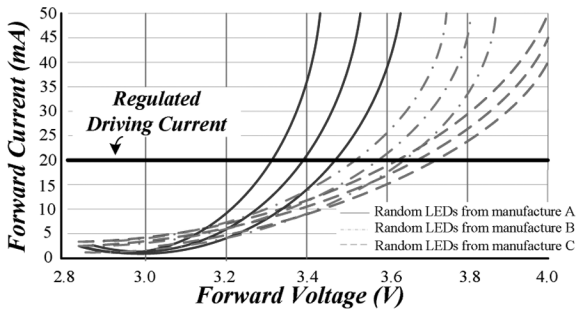

Fig. 2. I–V curve characteristic of LED.

Manuscript received May 12, 2009; revised June 25, 2009; acceptedJuly 13, 2009. First published December 18, 2009; current version published June 09, 2010. This work was supported by the National Science Council, Taiwan under Grant NSC 96-2221-E-009-240. This paper was recommended by Associate Editor H. S. Chung.

C.-H. Liu, C.-Y. Hsieh, Y.-C. Hsieh, and K.-Chen are with the Department of Electrical and Control Engineering, National Chiao Tung University, Hsinchu 30010, Taiwan (e-mail: khchen@cn.nctu.edu.tw).

T.-J. Tai was with the Department of Electrical and Control Engineering, National Chiao Tung University, Hsinchu 30010, Taiwan. He is now with Richtek Ltd., Guangzhou 510500, China.

Digital Object Identifier 10.1109/TCSI.2009.2028643

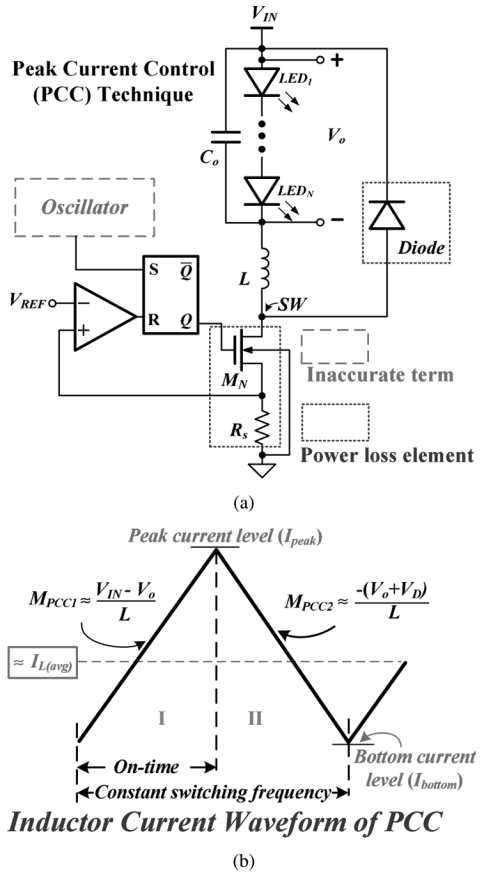

Fig. 3. Prior art for LED lighting system. (a) Implementation of the LED driver with the PCC technique. (b) Inductor current waveform of the PCC technique.

power MOSFET. As a result, the PCC technique has the advantage of high efficiency but low accuracy. Therefore, how to get high efficiency and accuracy at the same time becomes an important design issue in an LED lighting system. The proposed SAR-controlled adaptive off-time technique can achieve high accuracy and efficiency without any external sensing resistor.

This paper is organized as follows. Section II describes the operation of the prior arts of the LED drivers and discusses the advantages as well as the disadvantages of these prior arts. The design methodology of the proposed SAR-controlled adaptive off-time technique is described in Section III. Section IV shows the circuit implementations of the SAR-controlled adaptive off-time technique. Experimental results shown in Section V demonstrate how technique can achieve high accuracy LED current and improve the efficiency of the LED driver. Finally, conclusions are made in Section VI.

II. Fundamental Charging Process

The prior arts of the current regulator for LEDs contain two important control techniques. One is the PCC technique and the other one is the HCC technique [6].

A. Implementation of the Peak Current Control Technique

The implementation of the conventional PCC technique is shown in Fig. 3(a). It includes an oscillator to periodically turn on the N-type power MOSFET M_N. When the inductor current is increased to the predefined peak current level, the N-type power MOSFET M_N will be turned off. As a result, the inductor current is discharged by the freewheel-diode. The inductor current also flows through the LEDs; thus, the average inductor current will determine the brightness of the LEDs. Considering the inductor current waveform in the steady state as shown in Fig. 3(b), the inductor current ripple ΔI_L can be expressed as (1)

$$\Delta I_L = \frac{V_{\rm IN} - V_o}{L} t_{\rm on} = \frac{V_o + V_D}{L} t_{\rm off}$$

where

$$V_o \approx nV_F. \tag{1}$$

V_F and V_D are the forward voltages of the LED and the freewheel-diode, respectively. The V_o is equal to the summation of the total forward voltage of LED in series. The $t_{\rm on}$ and $t_{\rm off}$ are the on-time and off-time of the N-type power MOSFET M_N, respectively. Owing to the constant switching frequency, $t_{\rm on}$ and $t_{\rm off}$ can be approximately described as (2) and (3), respectively. The forward voltage of freewheel-diode is ignored in (2)

$$t_{\rm on} = DT_s = \frac{V_o}{V_{\rm IN}} T_s \tag{2}$$

$$t_{\rm off} = (1 - D)\, T_s = \left(1 - \frac{V_o}{V_{\rm IN}}\right) T_s. \tag{3}$$

T_s and D are defined as the switching period and the duty cycle of the LED driver, respectively [7]. Since the bottom current level is determined by the switching frequency, the average inductor current $I_{L(\rm avg.)}$ can be calculated as (4)

$$I_{L(\rm avg)} = I_{\rm peak} - \frac{V_o}{2L} t_{\rm OFF} = I_{\rm peak} - \frac{V_o T_s}{2L} \left(1 - \frac{V_o}{V_{\rm IN}}\right). \tag{4}$$

The value of the input voltage $V_{\rm IN}$ will affect the average inductor current. Moreover, the different numbers of LED in series which cause the different output voltage ($V_o \approx nV_F$) influence the average inductor current. Hence, the brightness of the LEDs is drastically influenced by the variation of the input voltage. Furthermore, as shown in Fig. 3(a), the major power dissipation of the LED driver in the PCC technique is caused by the external sensing resistor R_s and the diode during phases I and II, respectively. In phase I, the inductor current passes through the external sensing resistor R_s and the equivalent resistance of the $M_N(R_{\rm on})$ results in the energy consumption calculated as (5)

$$E_{phI(\rm PCC)} = I_{L(\rm avg)}^2 \times (R_{\rm on} + R_s) \times t_{\rm on}. \tag{5}$$

Moreover, the inductor current flows through the freewheel-diode to decrease the inductor current during phase II. Therefore, the freewheel-diode also brings the energy dissipation described as (6)

$$E_{phII(\rm PCC)} = I_{L(\rm avg)} \times V_D \times t_{\rm off}. \tag{6}$$

According to (5) and (6), the power consumption depends on the sensing resistor R_s and the forward voltage of freewheel-diode $V_{\rm Diode}$ because the R_s is much larger than $R_{\rm on}$. However, the power efficiency of the PCC technique is generally higher than the HCC technique because the inductor current passes through the sensing resistor during phase I instead of the full period.

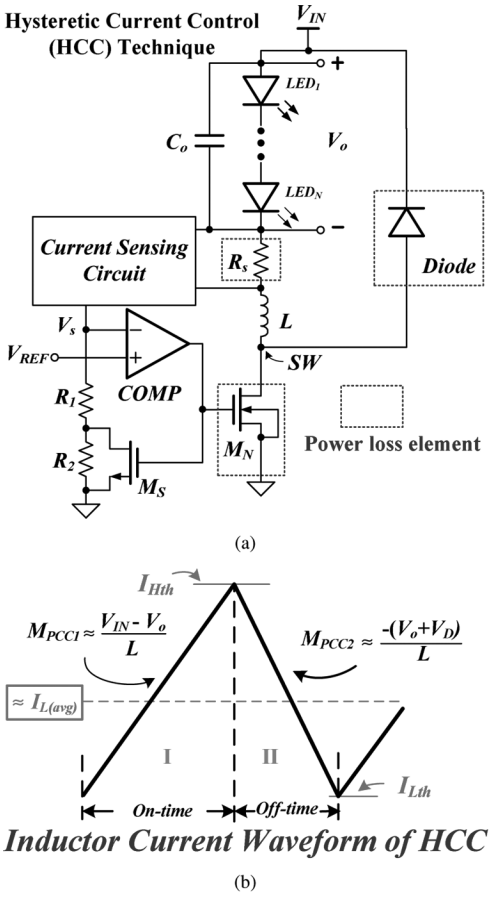

Fig. 4. Prior art for LED lighting system. (a) Implementation of the LED driver with the HCC technique. (b) Inductor current waveform of the HCC technique.

B. Implementation of the Hysteretic Current Control Technique

The HCC technique utilizes two threshold current levels to accurately control the average inductor current $I_{L(\mathrm{avg})}$, thereby defining the switching frequency [8]. The implementation of the fundamental HCC technique is shown in Fig. 4(a). It includes the simplest implementation of the current sensing circuit composed of an external resistor, R_S. The inductor current waveform in the steady-state is shown in Fig. 4(b). The two threshold current levels are defined as I_{Hth} and I_{Lth} indicating the high and low threshold current levels, respectively. When the switch M_S and the N-type power MOSFET M_N are turned on, the inductor current increases at a rate determined by $(V_{\mathrm{IN}} - V_o)/L$. Thus, the current sensing circuit generates the sensing current via R_1 and the switch M_S to produce the ramp voltage V_s. When the voltage V_s is higher than the V_{REF}, the switch M_S and the N-type power MOSFET M_N are turned off by the output of the comparator. Therefore, V_s has a step variation since the sensing current passes through both the resistors R_1 and R_2, not only through R_1. In addition, the inductor current is discharged via the freewheel-diode back to V_{IN}, as such, V_s decays at a rate decided by the inductor current. The current ripple can be defined as (7)

$$\Delta I_L = I_{Hth} \times \frac{R_2}{R_1 + R_2} = I_{Lth} \times \frac{R_2}{R_1}. \tag{7}$$

The HCC technique can accurately design the low threshold current I_{Lth} and the inductor current ripple by defining the high threshold current I_{Hth} and utilize the suitable resistors R_1 and R_2. Hence, the average inductor current can be accurately described as (8)

$$I_{L(\mathrm{avg})} = \frac{I_{Hth} + I_{Lth}}{2}. \tag{8}$$

As a result, the HCC technique can achieve a more accurate average current than that of the PCC technique. Hence, the brightness of the LEDs can be effectively controlled by the HCC technique. However, the large inductor current flows through the sensing resistor R_s in the full period since the whole switching period needs the information of the inductor current to compare it with the two threshold current levels. Thus, the energy dissipation by the conduction loss in phase I and phase II can be expressed as (9) and (10), respectively

$$E_{phI(\mathrm{HCC})} = I^2_{L(\mathrm{avg})} \times (R_{\mathrm{on}} + R_s) \times t_{\mathrm{on}} \tag{9}$$

$$E_{phII(\mathrm{HCC})} = \left(I_{L(\mathrm{avg})} \times V_D + I^2_{L(\mathrm{avg})} \times R_s\right) \times t_{\mathrm{off}}. \tag{10}$$

Comparing (6) and (10), the HCC technique produces another conduction loss due to the external sensing resistor during the phase II. Thus, the conduction loss of the HCC technique is larger than that of the PCC technique.

There is a tradeoff between accuracy and efficiency in the design of the LED driver. The HCC technique can have more accurate average current but larger conduction loss. On the other hand, the PCC technique can achieve higher efficiency at the expense of accuracy. To achieve higher accuracy and efficiency at the same time, the current regulator with the SAR-controlled adaptive off-time technique is proposed.

III. Design Methodology

The conduction loss of phase I due to the sensing resistor [9], [10] can be reduced by means of the on-chip low-side current sensing circuit that can accurately define the peak current level [11]. Additionally, the removal of the external sensing resistor can also save the cost and footprint area, but this causes an inability to sense inductor current during phase II [12]. Thereby, the average inductor current is difficult to accurately control because the bottom level of inductor current depend on the constant off-time or fixed frequency. Therefore, the accuracy of the LED lighting system is deteriorated. The value of the off-time needs to be adaptively adjusted to ensure the accurate inductor current that can be controlled between the peak and bottom current levels. As a result, the average inductor current can be independent of the variation of the input voltage and the numbers of LED in series. To adaptively adjust the value of the off-time [13], it is proposed that the SAR-controlled adaptive off-time calibrate the off-time value. That is, the duration of the off-time can be adjusted to regulate the bottom current level.

The flow chart of the SAR-controlled adaptive off-time technique is shown in Fig. 5. The 8-bit SAR code $A[7:0]$ is used to decide the duration of the off-time. At the beginning, the SAR code $A[7:0]$ has an initial value of "1000,0000" and the gain code $G[7:0]$ is set to "0100,0000". Adding or subtracting the gain code $G[7:0]$ leads to the accurate calibration values of the SAR code $A[7:0]$ in the following eight switching cycles. When the duration of the off-time is too short, the current

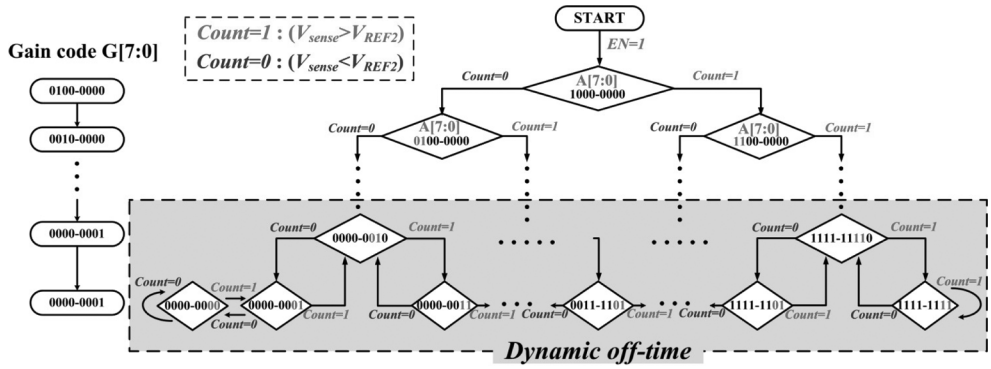

Fig. 5. Operation of the adaptive SAR code $A[7:0]$ by means of the gain code $G[7:0]$.

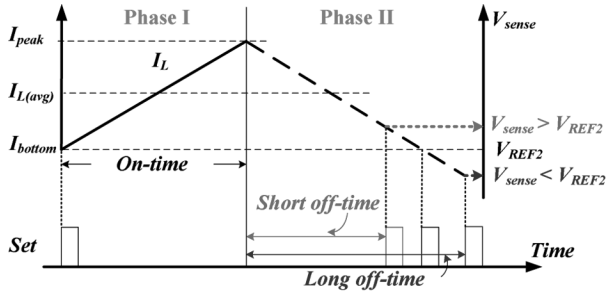

Fig. 6. Inductor current waveform at different the off-time values.

sensing signal $V_{\rm sense}$ at the beginning of the next switching cycle is larger than the expected value of $V_{\rm REF2}$ as shown in Fig. 6. Thus, the average inductor current is larger than expected value to have an influence on the brightness of the LED. At this time, the gain codes $G[7:0]$ would be added to the SAR code $A[7:0]$ to prolong the off-time. On the other hand, if the off-time is too long, the current sensing signal $V_{\rm sense}$ at the beginning of the next switching cycle will be smaller than the $V_{\rm REF2}$. That is, the lumen of LED is relatively small due to the smaller average inductor current, and therefore, the SAR code $A[7:0]$ will subtract the gain code $G[7:0]$.

After the eight switching cycles, the SAR code $A[7:0]$ can be dynamically adjusted by a minimum value of the gain code $G[7:0]$, which is "0000,0001," according to the value of the comparison result of the voltage $V_{\rm sense}$ and the reference voltage $V_{\rm REF2}$. Consequently, after the calibration duration, the adaptive off-time can ensure that the bottom level of the inductor current will be close to the expected value. That is, the average inductor current can be independent of the variation of the input voltage.

The external sensing resistor is not needed any more since the on-chip low-side current sensing circuit can detect the peak current level and the SAR code $A[7:0]$ adaptively adjusts the off-time. Therefore, the efficiency can be improved owing to the removal of the conduction loss of the external sensing resistor. Simultaneously, the accuracy is also guaranteed because the adaptive off-time can ensure the average inductor is independent of the variation of the input voltage. In other words, the SAR-controlled adaptive off-time has the advantages of high efficiency like the PCC technique and high accuracy like the HCC technique.

IV. Circuit Implementations

The implementation of the SAR-controlled adaptive off-time technique is illustrated in Fig. 7. The external sensing resistor is replaced by the on-chip low-side current sensing circuit. As a result, the power dissipation of the on-chip low-side current sensing circuit is much smaller than that of the external sensing resistor. Furthermore, the freewheel-diode [14] is substituted by the active diode, which is the P-type power MOSFET $M_{\rm Diode}$, in order to reduce the power dissipation during phase II. The digital signals *EN* and *CLR* are used to enable the LED driver and reset the initial digital code. The digital signal, *Digital PWM*, is the dimming signal for adjusting the brightness of the LED.

Two major circuits are used to enhance the accuracy of the LED driver. One is the SAR-controlled adaptive off-time control circuit and the other one is the on-chip low-side sensing circuit with the blanking time circuit. During phase I, the N-type power MOSFET is turned on to increase the inductor current. The current sensing circuit thus increases the sensing voltage $V_{\rm sense}$. Once $V_{\rm sense}$ is larger than $V_{\rm REF1}$, the output of the comparator "*CMP2*" triggers the signal *Reset* to turn off the N-type power MOSFET M_N. The on-time duration $t_{\rm on}$ is decided. The peak level of inductor current can be expressed as (11)

$$I_{\rm peak} = \frac{K \times V_{\rm REF1}}{R_{\rm sense}}. \tag{11}$$

K refers to the sensing ratio. At this particular time, the active diode $M_{\rm Diode}$ will be turned on to discharge the inductor current. The forward voltage of the active diode is the source-drain voltage V_{SD} of P-type power MOSFET. The off-time duration $t_{\rm off}$ is controlled by the 8-bit SAR code $A[7:0]$ from the SAR-controlled modulator. After the off-time duration, the adaptive off-time module sends a signal *Set* to turn on the N-type power MOSFET to charge the inductor current again.

At the beginning, the SAR-controlled adaptive off-time technique calibrates the off-time duration depending on the output "*Count*" of the comparator "CMP1". The signal "*Count*" equaled to "1" or "0" means that the sensing current signal $V_{\rm sense}$ is higher or lower than the reference voltage $V_{\rm ref2}$. After the calibration process, the bottom level of inductor current can be determined by the voltage $V_{\rm REF2}$. Thus, the bottom level of the inductor current can be formulated as (12)

$$I_{\rm bottom} = \frac{K \times V_{\rm REF2}}{R_{\rm sense}}. \tag{12}$$

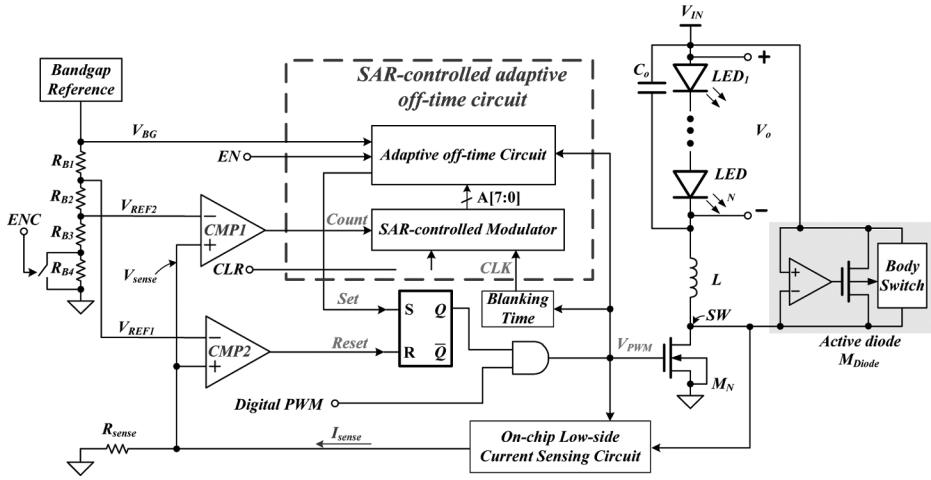

Fig. 7. Proposed LED current driver uses the SAR-controlled adaptive off-time technique.

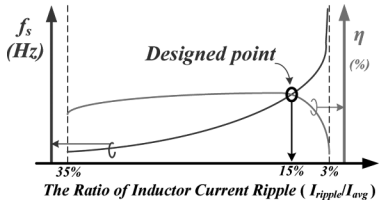

Fig. 8. Relation of the ratio of inductor current ripple $(I_{\rm ripple}/I_{\rm avg})$, the power efficiency (η), and the switching frequency (f_s).

Therefore, the current ripple divided by the average current can be calculated as (13)

$$\frac{I_{\rm ripple}}{I_{\rm avg}} = \frac{2\times(V_{\rm REF1}-V_{\rm REF2})}{(V_{\rm REF1}+V_{\rm REF2})}. \tag{13}$$

As a result, the current ripple ratio can be maintained by the reference voltages $V_{\rm ref1}$ and $V_{\rm ref2}$ and would not be influenced by the input voltage or the numbers of LED in series. Smaller current ripple has a more stable LED lumen. However, the ratio of the current ripple also defines the switching frequency as shown in (14)

$$f_s = \frac{1}{L\times I_{\rm ripple}\times\left(\frac{1}{V_o}+\frac{1}{V_{\rm IN}-V_o}\right)}. \tag{14}$$

According to (14), a small inductor current ripple results in a faster switching frequency and increases power consumption. On the other hand, a high inductor current ripple results in a slower switching frequency Therefore, power efficiency is increased because the switching loss is further reduced. However, the conduction power is increased due to large current ripple. Therefore, the inductor current ripple, which is about $\pm 15\%$ of the average inductor current has a better power conversion efficiency as shown in Fig. 8. The power efficiency would be reduced while the current ripple is smaller than $\pm 15\%$. Moreover, the current ripple can be increased to reduce the size of the inductor at the cost of reduced efficiency and, possibly, LED lifetime [15]. As a result, the suitable ratio of the inductor current ripple is $\pm 15\%$. This is popularly used in today's LED lighting products.

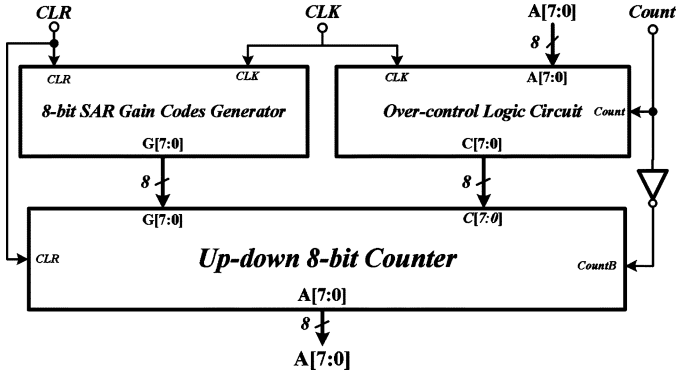

Fig. 9. Structure of the SAR-controlled modulator.

The LED driver needs to provide an accurate driving current for LED lighting systems. It should be noted that the SAR-controlled modulator can still dynamically adjust the off-time to rapidly react to the variations of the input voltage and the numbers of LED in series. In addition, the power dissipation during phases I and II can be reduced and expressed as (15) and (16), respectively

$$E_{phI(\rm SAR)} = I^2_{L(\rm avg)}\times R_{\rm on}\times t_{\rm on} \tag{15}$$

$$E_{phII(\rm SAR)} = I_{L(\rm avg)}\times V_{SD}\times t_{\rm off}. \tag{16}$$

According to (11), the power dissipation in phase I is much less than those in (5) and (9). During phase II, the power dissipation can also be reduced through the use of small $V_{\rm DS}$ because of the active diode. Hence, the technique can minimize the conduction power loss and improve the accuracy of the driving current. Sections IV-A–IV-C will describe the implementations of the sub-modules.

A. Implementation of the SAR-Controlled Modulator

The implementation of the SAR-controlled modulator is composed of three sub-modules as shown in Fig. 9. The three sub-modules are the up-down 8-bit counter, the 8-bit SAR gain code generator, and the over-control logic circuit. The up-down 8-bit counter is used to calculate a new 8-bit SAR code $A[7:0]$ and a gain code $G[7:0]$ according to the digital signal *Count*.

The 8-bit SAR gain code generator provides $G[7:0]$ to the up-down 8-bit counter to calculate the precise $A[7:0]$. The over-control logic circuit detects $A[7:0]$ and generates $C[7:0]$ to avoid the overflow issue.

The circuit of the up-down 8-bit counter is the main module shown in Fig. 10(a). Since $A[7:0]$ starts from "10000000", the gate DFF8 utilizes the complement of the Q signal when the signal *CLR* is high. Therefore, $A[7:0]$ starts from "10000000" after the clear state. The eight XOR gates and the signal *CountB* are used to decide if the operation is an addition or a subtraction. Additionally, *CountB* is also used as the carry-in signal of the first full-adder to achieve the correct calculation. When *CountB* is "1", $G[7:0]$ will be converted into its 2's complement value. Hence, $A[7:0]$ subtracts $G[7:0]$ to prolong the off-time duration. On other hand, if *CountB* is "0", $G[7:0]$ is not complemented. That is, the addition is proceeded by the SAR-controlled modulator and $A[7:0]$ is equal to the sum of the previous value and $G[7:0]$.

The 8-bit gain code generator is shown in Fig. 10(b). $G[7:0]$ starts from "01000000" to "00000001". At the beginning, the binary code $[\mathrm{out2}, \mathrm{out1}, \mathrm{out0}]$ is set to "000" and converted by the 3-to-8 decoder so that $G[7:0]$ can be set as "01000000". Three full adders are used to generate the increasing binary code $[\mathrm{out2}, \mathrm{out1}, \mathrm{out0}]$ from "000" and $G[7:0]$ is converted from "01000000" to "00000001" by the 3-to-8 decoder. Until $G[0]$ is changed from "0" to "1", the input B of the full adder I becomes "0" and the binary code $[\mathrm{out2}, \mathrm{out1}, \mathrm{out0}]$ will be settled. This indicates the end point of the calibration of the SAR operation. Then, the SAR-controlled modulator starts to slightly adjust $A[7:0]$ by setting the minimum $G[7:0]$ as "00000001".

The over-control logic circuit is depicted in Fig. 10(c). The AND gate array is used to block the clock *CLK* when the overflow issue happens. When the value of the signal *CountB* is "1", the operation of the up-down 8-bit counter is the addition function. If $A[7:0]$ is "11111111", the output of the XOR gate array is "0" to block the clock signal *CLK*. Thus the over-control signal $C[7:0]$ holds to "00000000". For the subtraction function, the up-down 8-bit counter needs to prevent the value of the SAR code $A[7:0]$ from continuously decreasing when $A[7:0]$ is "00000000". When the function of subtraction is enabled by the *CountB*, it also prevents the overflow issue from happening through the XOR gate array. The SAR-controlled modulator with three sub-modules can generate $A[7:0]$ through the digital signal *Count* to adjust the dynamic off-time. When *Count* is "0" or "1", the SAR code will subtract or add $G[7:0]$ as "00000001".

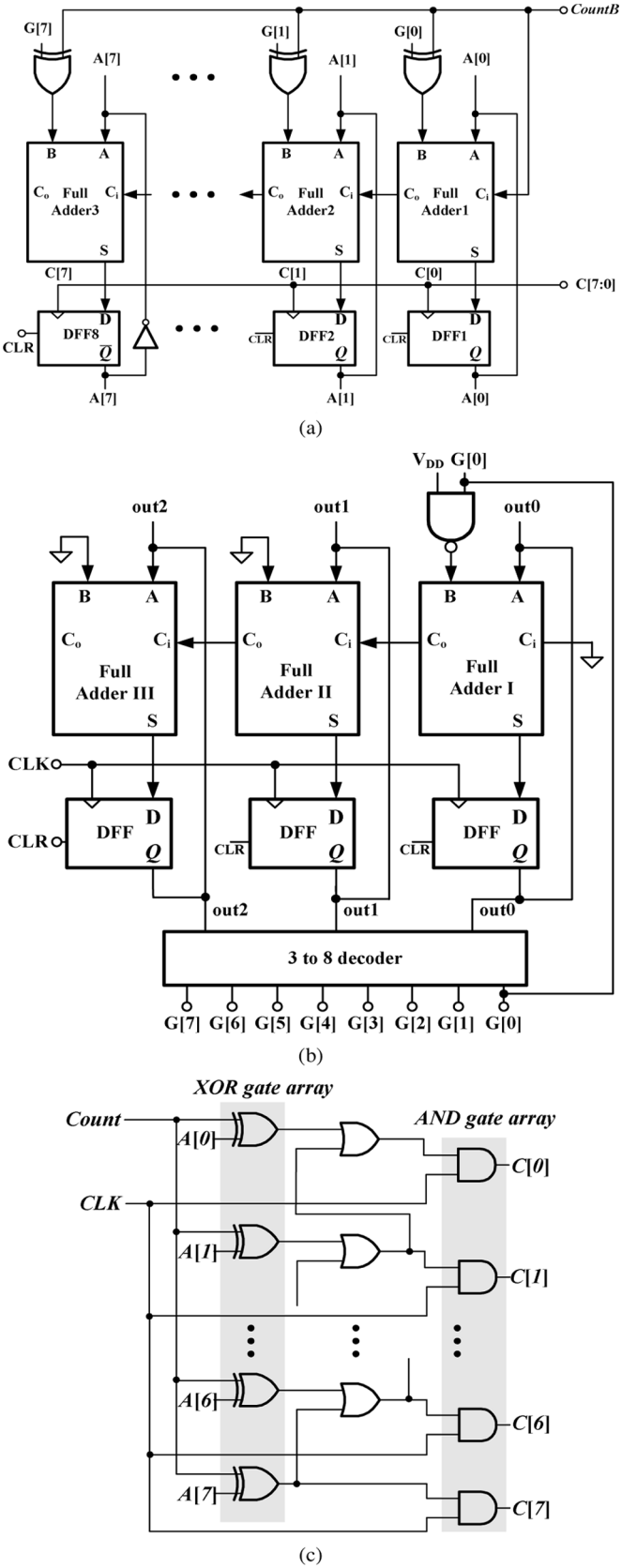

Fig. 10. Three sub-modules in the implementation of the SAR-controlled modulator. (a) Up-down 8-bit counter. (b) 8-bit SAR gain code generator. (c) Over-control logic circuit.

B. Implementation of the Adaptive Off-Time Circuit

The simple implementation of the constant off-time circuit is depicted in Fig. 11(a). When the signal *control* is high, the non-inverting input of comparator V_{ca} is discharged to ground and the output of comparator *Set* is zero. When the signal *control* is changed to low, the constant biasing current I_B will flow into the capacitor C_{off} to increase V_{ca}. Once V_{ca} is larger than the voltage V_{BG}, the signal *Set* is changed to high to start the next switching cycle. Thus, the off-time duration can be expressed as (17)

$$t_{\mathrm{off}} = \frac{C_{\mathrm{off}} V_{BG}}{I_B} \tag{17}$$

where t_{off} is proportional to the value of the capacitor C_{off}. Therefore, the adaptive off-time circuit as illustrated in

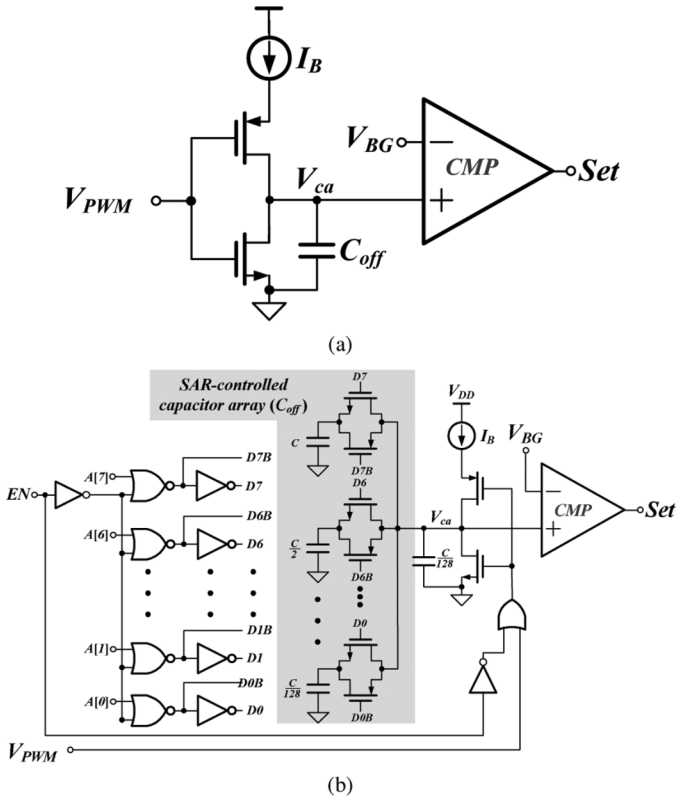

Fig. 11. (a) Implementation of a simple off-time circuit. (b) Schematic of the adaptive off-time circuit and the corresponding capacitor according to each bit of the SAR code $A[7:0]$.

Fig. 11(b) utilizes the SAR codes to adjust the value of the capacitor for the suitable off-time $t_{\rm off}$. $A[7:0]$ turns on/off the switches in the SAR-controlled capacitor array to decide the total value of $C_{\rm off}$ when the input enable signal *EN* is high. Each bit in $A[7:0]$ indicates the additional capacitor. As such, $C_{\rm off}$ can be expressed as (18)

$$C_{\rm off} = C \times (2^0 \cdot A_7 + 2^{-1} \cdot A_6 + \cdots + 2^{-7} \cdot A_0 + 2^{-7}). \quad (18)$$

Thus, the maximum and minimum values of the capacitor are $2C$ and $C/128$, respectively. As a result, the off-time $t_{\rm off}$ can be dynamically adjusted to get the accurate average inductor current.

C. Implementation of the On-Chip Low-Side Current Sensing and the Blanking Time Circuits

The on-chip low-side current sensing circuit is shown in Fig. 12. The switches $M_{s1} - M_{s3}$ are used to control the turning on/off the current sensing mechanism. When the $V_{\rm PWM}$ changes to high to turn on the N-type power MOSFET M_N, the sensing MOSFET $M_{\rm sense}$, and the switch M_{s1}, the voltage at node *SW* will pass to V_B through the M_{s1} and voltage $V_{\rm A}$ will be equal to the voltage at node *SW* due to the close-loop of the amplifier. Thus, the transistors M_N and $M_{\rm sense}$ will have the same drain, gate, source, and bulk voltages. The W/L ratio of M_N to $M_{\rm sense}$ is about K. In this design, the value of K is 3000. The current I_s is approximately equal to $(1/3000) \times I_L$. The inductor current information passes through the current

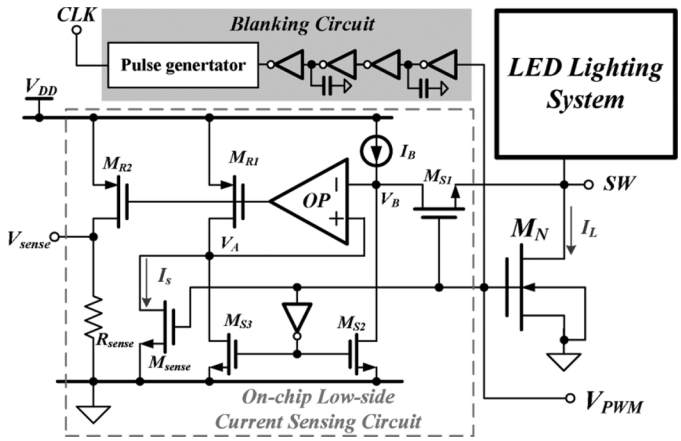

Fig. 12. Design of the on-chip low-side current sensing circuit with the blanking time circuit.

mirror pair, composed of transistors $M_{\rm R1}$ and $M_{\rm R2}$, to generate the sensing signal $V_{\rm sense}$, which is used to compare two reference voltages, $V_{\rm REF1}$ and $V_{\rm REF2}$, to decide the values of $t_{\rm on}$ and $t_{\rm off}$.

At the beginning of every switching cycle, the current sensing signal $V_{\rm sense}$ is utilized to determine whether the digital *Count* is "1" or "0". Since the clock signal *CLK* in the SAR-controlled modulator can trigger the calibration of the off-time duration, $V_{\rm sense}$ needs to correctly present the inductor current information before the clock signal *CLK* changes from low to high. Thus, the blanking time circuit is used to delay the signal $V_{\rm PWM}$ to generate the clock signal *CLK*. That is, the blanking time circuit provides enough time for $V_{\rm sense}$ to track the variation of the load current. Therefore, $A[7:0]$ can accurately decide the value of the capacitor.

V. Experimental Results

The proposed SAR-controlled adaptive off-time technique for the LED lighting systems was fabricated by the UMC 0.35-μm high voltage process. The threshold voltages of n-type and p-type low voltage MOSFET are 0.56 and 0.79 V, respectively. The chip micrograph is shown in Fig. 13(a). The total silicon area including the testing pad is about 1100 μm$\times$ 1000 μm. The developed prototype is shown in Fig. 13(b). The LED current driver in this technique can operate from 8 to 40 V and the regulated driving current can be higher at about 1 A. The detailed specifications are listed in Table I. The maximum adaptive off-time is about 2.5 μs and the duty is about 5% when the input voltage is 40 V and the load is one LED. If the input voltage is at 20 V and the load is 8 LEDs, the LED driver will continuously turn on the N-type power MOSFET but the input voltage cannot overcome the forward voltage of 8-LEDs. As a result, the switching frequency is zero and duty ratio cannot be defined. The off-time stays at the initial value. That is, the off-time value is well-defined at all conditions.

The on-chip reference voltage can be adjusted to 360 and 720 mA and the experimental results are shown in Fig. 14(a) and (b), respectively. The SAR-controlled adaptive off-time technique starts to calibrate the off-time duration once the LED driver is enabled. After eight switching clock cycles, the off-time value

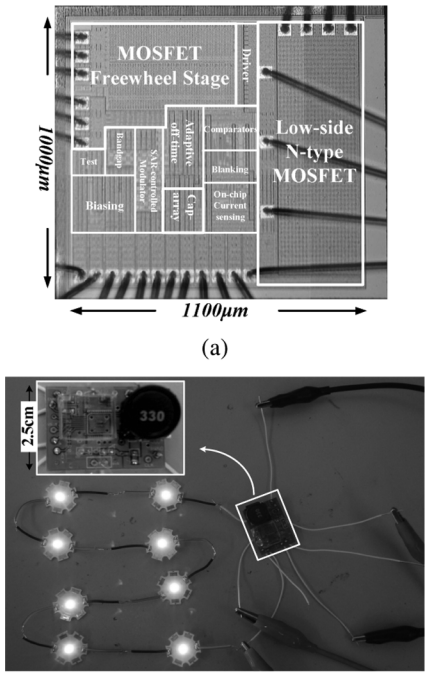

Fig. 13. (a) Chip micrograph. (b) Prototype for testing the LED driver.

TABLE I
SPECIFICATION

Fabrication Process	UMC 0.35μm high voltage process
Chip area	1100μm*1000μm
V_{IN}	8V to 40V
Supply Voltage	4V
Quiescent current	0.5mA
Maximum adaptive off-time	2.5 μs
SW	8V to 40V
Inductor	33μH
Maximum LED Current	1.5A

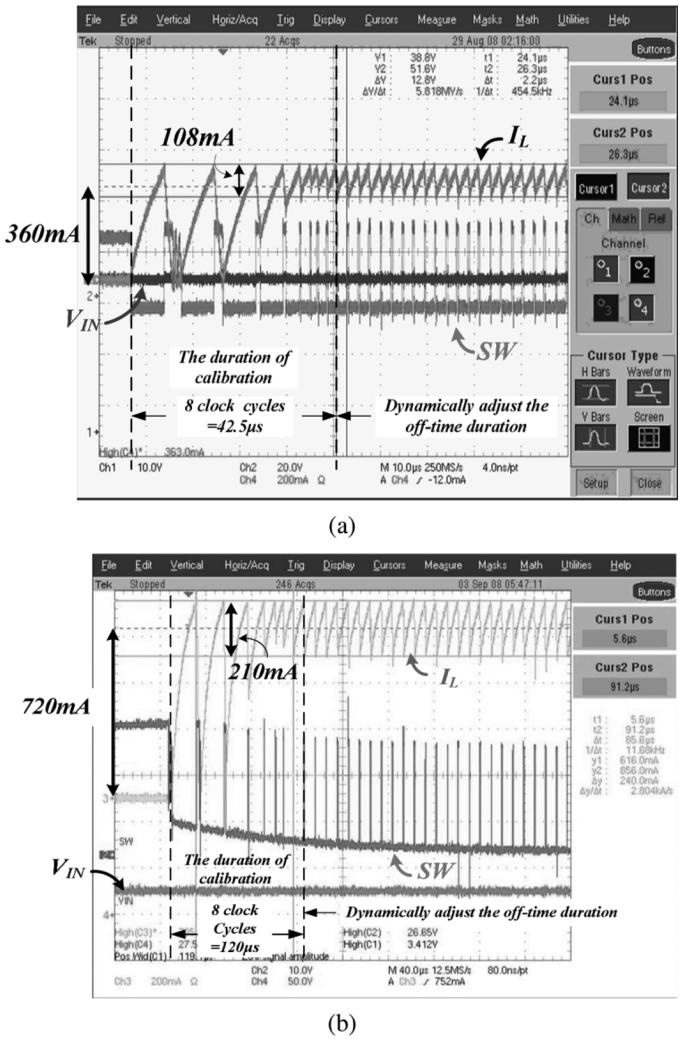

Fig. 14. Experimental results show the adaptive off-time is determined after 8 clock cycles by the SAR-controlled adaptive off-time technique when the LED driving currents are (a) 360 and (b) 720 mA.

is determined and this technique enters the dynamic adjustment stage through the up-down converter. In particular, t_{off} is finely and adaptively adjusted for the variation of the environment after the calibration stage. The calibration times are 42.5 and 120 μs when the LED driving currents are 360 and 720 mA, respectively. The average inductor currents are adjusted to the predefined values of 360 and 720 mA. After the calibration, the ripples of the inductor current (I_L) are adjusted to 108 and 210 mA peak-to-peak when the LED driving currents are 360 and 720 mA, respectively. The inductor current ripple is approximated to within $\pm 15\%$ of the average inductor current. The switching frequencies of the two load conditions are different because of the adaptive off-time.

Fig. 15(a) demonstrates that this technique can rapidly adjust the off-time t_{off} to maintain the LED driving current when the input voltage is increased from 10 to 20 V and vice versa. Furthermore, the digital PWM signal is used to adjust the brightness of the LED lighting system at different duties of the digital PWM. The inductor current operates at the defined value when the digital PWM signal is high. In addition, the inductor current is zero when the digital PWM signal is low. Thus, the average output current can be adjusted between 0% and 100% by adjusting the duty ratio of the digital PWM signal. Similarly, when the number of LEDs is changed, the condition is the same as the test of line transient regulation because the voltage across the inductor is changed and the LED current is kept constant. As shown in Fig. 15(b), the average current can also be maintained at 720 mA by the dynamic off-time when the duty of PWM dimming is 100% and the input voltage is increased from 10 to 20 V and vice versa. That is, the proposed SAR-controlled adaptive off-time technique can adjust the off-time depending on the input voltage and the number of LEDs. Fig. 15(c) shows the experimental results of the inductor current waveforms when the duties of the digital PWM signal are 25% and 50%. The average inductor current is adjusted back to the predefined 720 mA after eight switching cycles at the beginning of the digital PWM signal. This technique can effectively adjust the off-time t_{off} back to its accurate value every time when the LED lighting system is turned on.

Fig. 16(a) demonstrates the improvement of the power conversion efficiency compared with the previous designs. The power conversion efficiency is increased by about 8%–15%

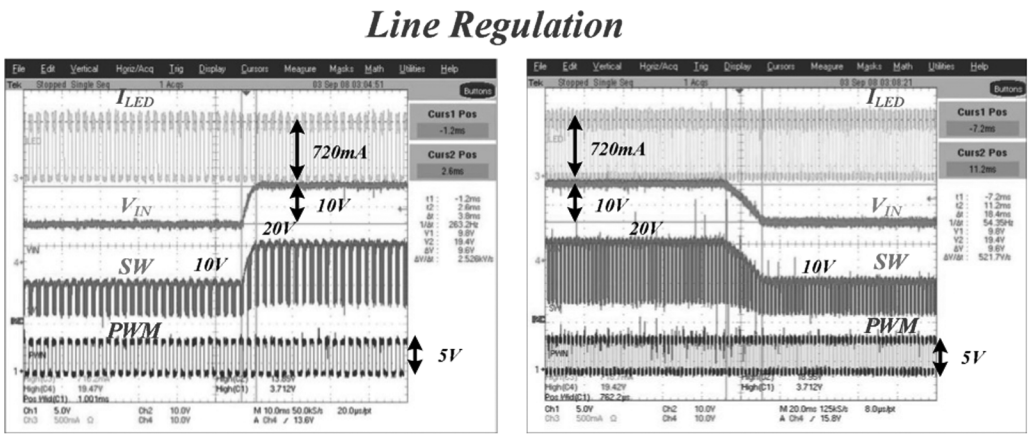

(a)

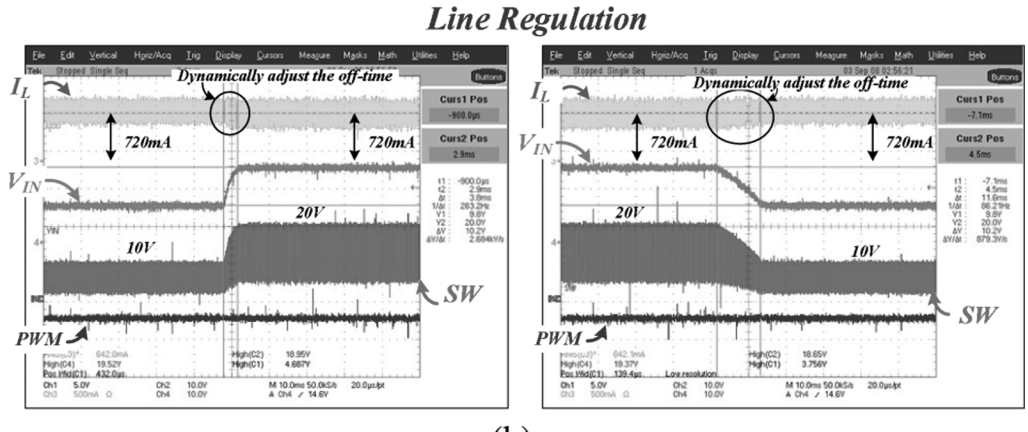

(b)

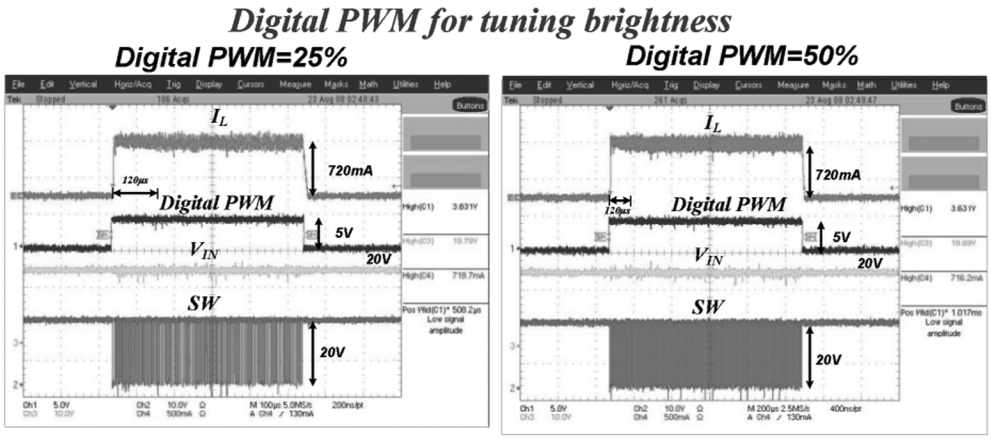

(c)

Fig. 15. Experimental results. (a) Waveforms of the performance of line regulation when the duty of the PWM dimming is 50% and the input supply voltage changes from 10 to 20 V or vice versa. (b) Waveforms of the performance of line regulation when the duty of PWM dimming is 100% and the input supply voltage changes from 10 to 20 V or vice versa. (c) Waveforms of the SAR-controlled adaptive off-time technique when the duties of the digital PWM signal are 25% and 50%.

compared to the HCC method, and by about 5%–8% compared to the PCC method when the LED driver is used to drive 5 to 8 series-LEDs. As shown in Fig. 16(b), the accuracy of this proposed technique can only keep 1% error percentage compared to that of the HCC technique. However, the error percentage of the PCC method may be larger than 15% under different input supply voltages. In other words, the SAR-controlled adaptive off-time technique can effectively enhance the power conversion efficiency and, at the same time, provide accurate driving current. Fig. 17 shows the comparison of the error percentages under different input voltage and temperature when the LED driver is used to drive 5 series-LEDs. The error percentage of the PCC and HCC technique is about 11.27% and 1.06%, respectively. The proposed SAR-controlled adaptive off-time method can keep a low error percentage, which is about 1.37%, as low as the HCC technique. Fig. 18 shows the

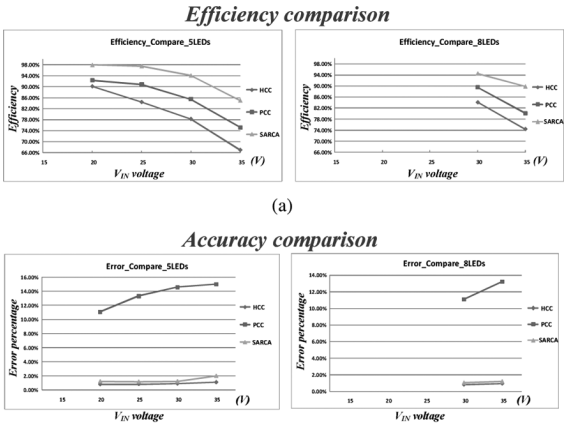

Fig. 16. Experiment results. (a) Efficiency comparison between the HCC, PCC and SAR-controlled adaptive off-time techniques when the LED driver is used to drive 5 to 8 series-LEDs. (b) Accuracy comparison between the HCC, PCC, and SAR-controlled adaptive off-time techniques at different input supply voltages.

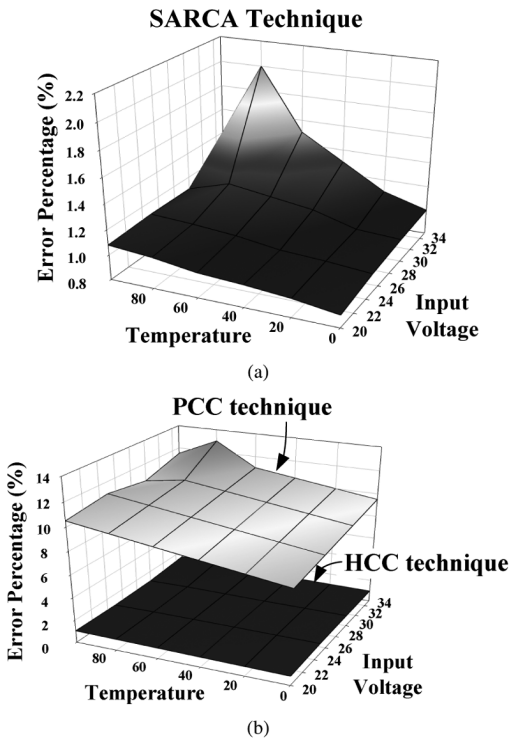

Fig. 17. Comparison of error percentages under different input voltage and temperature when the LED driver is used to drive 5 series-LEDs. (a) Results of the proposed SARCA method. (b) Results of the PCC and HCC methods.

estimated results of 200 samples with different temperatures. The average current is 720 mA. The standard deviation is 2 mA and the coefficient of variation is 0.28%. The temperature coefficient was less than 50 ppm/°C. Consequently, the proposed technique can achieve high accuracy without being affected by the variations of the input voltage and temperature.

The comparison between the proposed technique with the HCC and PCC techniques is listed in Table II. The proposed SAR-controlled adaptive off-time technique can achieve 94% efficiency and 98% accuracy for LED lighting system.

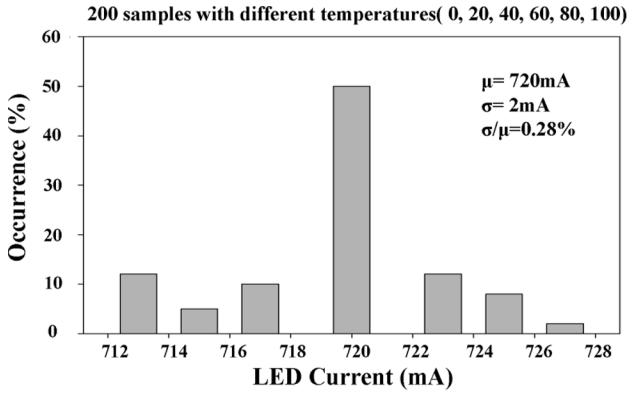

Fig. 18. Distribution in 200 samples with different temperatures.

TABLE II
COMPARISON WITH OTHER TECHNIQUES

	SAR-controlled	HCC	PCC
Sensing resistor	*NO*	*YES*	*YES*
Line regulation error	*2%*	*2%*	*<17%*
Current error percentage	*2.01%*	*1.11%*	*23%*
Efficiency	*94.3 %*	*82.9 %*	*88.2 %*

VI. CONCLUSION

The prior arts of the LED drivers such as the PCC and HCC methods have shown a trade-off between efficiency and accuracy. In this paper, the LED driver with the SAR-controlled adaptive off-time technique is proposed to achieve high accuracy and efficiency at the same time. According to the operation of this technique, the average inductor current can be adjusted to a constant value. The on-chip low-side current sensing method and the active diode can greatly improve efficiency. Thus, this topology achieves 94% efficiency and 98% accuracy. The power efficiency is increased to about 8%–15% compared to the HCC method and to about 5%–8% compared to the PCC method. The SAR-controlled adaptive off-time technique can be widely used in LED lighting systems with PWM dimming control.

REFERENCES

[1] B. R. Rae, C. Griffin, K. R. Muir, J. M. Girkin, E. Gu, D. R. Renshaw, E. Charbon, M. D. Dawson, and R. K. Henderson, "A microsystem for time-resolved fluorescence analysis using CMOS single-photon avalanche diodes and micro-LEDs," in *IEEE ISSCC Dig. Tech. Papers*, Feb. 2008, pp. 166–603.

[2] I.-H. Oh, "A single-stage power converter for a large screen LCD backlighting," in *Proc. IEEE APEC*, Mar. 2006, pp. 1058–1063.

[3] C.-C. Chen, C.-Y. Wu, and T.-F. Wu, "LED back-light driving system for LCD panels," in *Proc. IEEE APEC*, Mar. 2006, pp. 381–385.

[4] H.-J. Chiu and S.-J. Cheng, "LED backlight driving system for large-scale LCD panels," *IEEE Trans. Ind. Electron.*, vol. 54, no. 10, pp. 2751–2760, Oct. 2007.

[5] Y.-J. Jeon, Y.-S. Son, J.-Y. Jeon, and G.-H. Cho, "Improved transient current feedforward output buffer for fast and comapct active-matrix OLED column drivers," *IEEE Trans. Circuits Syst. II, Analog Digit. Signal Process.*, to be published.

[6] I.-H. Oh, "An analysis of current accuracies in peak and hysteretic current controlled power LED drivers," in *Proc. IEEE APEC*, Feb. 2008, pp. 572–577.

[7] R. W. Erickson and D. Maksimovic, *Fundamentals of Power Electronics*. Norwell, MA: Kluwer, 2001.

[8] R. D. Middlebrook, "Modeling current-programmed buck and boost regulators," *IEEE Trans. Power Electron.*, vol. 4, no. 1, pp. 36–52, Jan. 1989.

[9] Maxim Integrated Products, Inc., Maxim, CA, "MAX16807/MAX16808: Integrated 8-channel LED drivers with switch-mode boost and SEPIC controller," Datasheet, 2007.
[10] Intersil Corp., CA, "Powering LED strings and arrays in backlight applications," Appl. Note EL7801, 2006.
[11] C. Y. Leung, P. K. T. Mok, and K. N. Leung, "A 1-V integrated current-mode boost converter in standard 3.3/5-V CMOS technologies," *IEEE J. Solid-State Circuits*, vol. 40, no. 11, pp. 2265–2274, Nov. 2005.
[12] H. van der Broect, G. Sauerlander, and M. Went, "Power driver topologies and control schemes for LEDs," in *Proc. IEEE APEC*, Mar. 2007, pp. 1319–1325.
[13] G. Zhang, S. Saw, J. Liu, S. Sterrantino, D. K. Johnson, and S. Jung, "An accurate current source with on-chip self-calibration circuits for low-voltage current-mode differential drivers," *IEEE Trans. Circuits Syst. I, Fundam. Theory Appl.*, vol. 53, no. 1, pp. 40–47, Jan. 2006.
[14] K. Sung and L.-S. Kim, "A high-resolution synchronous mirror delay using successive approximation register," *IEEE J. Solid-State Circuits*, vol. 39, no. 11, pp. 1997–2004, Nov. 2004.
[15] Supertex Inc., CA, "Buck-based LED drivers using the HV9910B," Appl. Note, 2005.

Chao-Hsuan Liu was born in Hsinchu, Taiwan. He received the B.S. degree in electrical engineering from Nation Chung Hsing University, Taichung, Taiwan, in 1998, and the M.S. degree in electrical engineering from Nation Chiao Tung University, Hsinchu, Taiwan, in 2007.

He is an analog designer with ITE Tech. Inc., Hsinchu, Taiwan. His research interests contain many projects of LED driver ICs and power management ICs at mixed-signal and power management IC Laboratory in Nation Chiao Tung University.

Chun-Yu Hsieh was born in Taichung, Taiwan. He received the B.S. degree in electrical and control engineering from Nation Chiao Tung University, Taiwan, in 2006, where he is currently pursuing the Ph.D. degree in electrical and control engineering.

His research interests include many projects of LED driver ICs and power management ICs at Mixed-Signal and Power Management IC Laboratory. His interests include power management circuit designs, LED driver ICs, and analog integrated circuit designs.

Yu-Chiao Hsieh He was born in Hsinchu, Taiwan. received the B.S. degree in Electrical and Control Engineering from National Chiao Tung University, Taiwan, in 2007, where he is pursuing the Ph.D. degree in the Department of Electrical and Control Engineering.

His research interests include LED drivers and power management ICs.

Ting-Jung Tai was born in Hsinchu, Taiwan, in 1983. He received the B.S. degree and the M. S. degree from the Electrical and Control Engineering Department, National Chiao Tung University, Hsinchu, Taiwan, in 2006 and 2008, respectively.

He is with Richtek, Ltd., Guangzhou, China. His research interests include the current sharing technique and DC-DC converters at Low Power Mixed Signal Lab. His research interests are also in DC-DC converters, current sharing technique and analog integrated circuit design.

Ke-Horng Chen (M'04–SM'09) received the B.S., M.S., and Ph.D. degrees in electrical engineering from National Taiwan University, Taipei, Taiwan, in 1994, 1996, and 2003, respectively.

From 1996 to 1998, he was a part-time IC Designer at Philips, Taipei. From 1998 to 2000, he was an Application Engineer at Avanti, Ltd., Taiwan. From 2000 to 2003, he was a Project Manager at ACARD, Ltd., where he was engaged in designing power management ICs. He is currently an Associate Professor in the Department of Electrical Engineering, National Chiao Tung University, Hsinchu, Taiwan, where he organized a Mixed-Signal and Power Management IC Laboratory. He is the author or coauthor of more than 80 papers published in journals and conferences, and also holds several patents. His current research interests include power management ICs, mixed-signal circuit designs, display algorithm and driver designs of liquid crystal display (LCD) TV, red, green, and blue (RGB) color sequential backlight designs for optically compensated bend (OCB) panels, and low-voltage circuit designs.